

# Synthetic aperture holography: a novel approach to three-dimensional displays

Pierre St. Hilaire, Stephen A. Benton, and Mark Lucente

*Spatial Imaging Group, MIT Media Laboratory, Room E15-422, 20 Ames Street, Cambridge, Massachusetts 02139*

Received October 30, 1991; revised manuscript received April 28, 1992; accepted May 12, 1992

We describe an electro-optic apparatus capable of displaying a computer-generated hologram in real time. The computer-generated hologram is calculated by a supercomputer, read from a fast frame buffer, and transmitted to a wide-bandwidth acousto-optic modulator. Coherent light is modulated by the acousto-optic modulator and optically processed to produce a three-dimensional image with horizontal parallax. We evaluate different display geometries and their effect on the optical parameters of the system. We then show how the display resolution can be increased by simultaneously writing three acoustic columns on a single crystal and optically multiplexing the resulting holograms. We finally describe some improvements that follow from the analysis.

## 1. INTRODUCTION

Holography has long been recognized as an effective way to convey the information of complex three-dimensional structures such as those encountered in medical imaging, computer-aided design, and navigation. Conventional display holograms can produce bright, full-color images of high resolution and with a large range of depths but cannot be altered electronically as can typical two-dimensional displays. Attempts at implementing a real-time holographic display device have been hampered by the requirement for enormous space-bandwidth products for their implementation. As a result, a large body of literature exists concerning the computer generation of holograms,<sup>1,2</sup> but few attempts have been made to display such holograms at near-video frame rates. Holograms that are displayed by using present-generation liquid-crystal display or magneto-optic light valves have a space-bandwidth product that is too small by at least 2 orders of magnitude to qualify as display holograms, and devices that use scanned laser or electron beams to write the fringes are too slow for practical applications. We present here an approach based on the use of acousto-optic (AO) technology in which the active display medium consists of an AO crystal whose image is scanned across the display area in a raster scan fashion. Such an approach alleviates many of the problems encountered in previous attempts at real-time computer-generated holography.

We describe the bandwidth problem in Section 2 and then give an overview of the system in Section 3. Section 4 gives a more mathematically detailed description of the display and a discussion of image resolution. Signal processing issues are discussed in Section 5, and Section 6 introduces the use of multichannel acousto-optic modulators (AOM's). We then describe the results obtained so far and discuss some possible future directions for our research.

## 2. OVERCOMING THE BANDWIDTH BOTTLENECK

It was realized early that the limited information bandwidth available in electronic, computing, and communica-

tion systems would severely handicap progress toward real-time holography.<sup>3-5</sup> The information content of a holographic image is readily calculated if we start from the grating equation:

$$f_h \lambda = \sin \theta, \quad (1)$$

where  $f_h$  is the maximum spatial frequency of the hologram fringes,  $\lambda$  is the wavelength of the diffracted light, and  $\theta$  is the angular width of the view zone.

According to the sampling theorem, the minimum sampling frequency  $f_s$  required for generation or digital transmission of the hologram is

$$f_s = 2f_h, \quad (2)$$

so that the number  $N$  of samples required for a one-dimensional hologram of width  $d$  is

$$N = df_s = \frac{2d \sin \theta}{\lambda}. \quad (3)$$

The total number  $N_t$  of samples required for a hologram with only horizontal parallax and with a vertical resolution of  $l$  lines is thus

$$N_t = lN_s = \frac{2dl \sin \theta}{\lambda}. \quad (4)$$

For a full parallax hologram of height  $w$  we have

$$N_t = \frac{4dw \sin^2 \theta}{\lambda^2}. \quad (5)$$

The information content of a typical hologram is thus several orders of magnitude larger than that of a two-dimensional image, such as the image on a CRT display. From Eq. (5), a full parallax hologram that is 100 mm  $\times$  100 mm and has a maximum diffraction angle of 30° contains approximately  $25 \times 10^9$  samples of information, all for a single frame. To update such an image with

8-bit resolution at a rate of 60 frames/s, a data rate of 12 Tbits/s would be required for transmission of the hologram. This bandwidth is well beyond the range of current technology.

At the Spatial Imaging Group we have taken several steps to reduce the information content of holograms to a level that could be realized with the existing technology. First, the vertical parallax has been eliminated from the computer-generated hologram (CGH) before computation, reducing the information content by several orders of magnitude. The resulting hologram is similar to the rainbow hologram, which trades vertical look-around for ease of viewing.<sup>4</sup> Second, the horizontal field of view has been limited to 15°, permitting only a few standard eye spacings at an arm's length. Third, the resolution of the image has been reduced to the visual limit or the resolution of the data. With such an approach, and using Eq. (4), a 5 cm × 5 cm image with a 15° field of view, and 100 horizontal lines, we reduce the data requirements to  $4.1 \times 10^6$  samples per frame, or 2 Gbits/s of bandwidth, assuming a 60-Hz refresh rate. Such a data rate is within the capabilities of existing technology, although it nonetheless presents a challenge. This number can be decreased further if we allow for a lower frame rate or other informational economies.

### 3. OVERVIEW OF THE MIT DISPLAY

The fundamental idea behind the MIT holovideo display is the use of an AOM as the medium upon which the holograms are written.<sup>5,6</sup> The AOM consists of a single transparent TeO<sub>2</sub> crystal operated in the slow shear mode. At one end of the crystal is an ultrasonic transducer, which converts the electrical holographic information signal to a shear wave that is launched down the crystal. As the shear wave propagates, the regions of greater elastic shear present a modulated index of refraction to the optical beam, which passes at the Bragg angle with respect to the acoustic wave. The optical beam thus emerges from the crystal with a relative phase-difference pattern across its width that is proportional to the instantaneous amplitude of the shear wave along the length of the crystal. This complex fringe pattern transfers the CGH data to the optical beam. The crystal has an aperture time (width/sound speed) of 40 μs and a space-bandwidth product (max cycles/mm × aperture width) of 2000. Its operating rf spectrum ranges from 50 to 100 MHz. Because its total angle of diffraction range is only 3°, optical demagnification is needed to bring the viewing angle to a more acceptable value (typically 15°).

Figure 1 shows the electro-optic portion of the display. A widened beam of coherent light is phase modulated by the input CGH data stream in the AOM and assembled into the image of the CGH by the scanning system. A 10-mW He-Ne laser is used as a coherent source of monochromatic red light (632.8-nm wavelength). The beam is spatially filtered, expanded, and collimated by a microscope objective, a pinhole, and a collimating lens. A horizontal slit-shaped portion of this beam passes through the AOM, producing a diffracted order, which represents a portion of one line of the hologram. In the AOM, the fringes propagate at a rate of 617 m/s, which is the speed of shear waves in the TeO<sub>2</sub> crystal. Therefore the diffracted

image also moves (from left to right) at this rate. To make the image appear stationary, a spinning polygonal mirror is used to scan the image of the AOM horizontally in the opposite direction. The horizontal scan also acts to multiplex the image of the crystal, creating a virtual crystal that is exactly as long as one line of the CGH. This multiplexing is necessary because the crystal's time-bandwidth product is typically at least an order of magnitude smaller than the time-bandwidth product of a single hologram line. We can thus think of our CGH as a narrow slit being displaced along a much wider hologram. This situation is similar to the synthetic aperture radar (SAR) case, in which a narrow antenna is linearly and coherently scanned to give an effective aperture equal to the scan length, the main difference being that we are generating a wave front instead of recording one (thus the name synthetic aperture holography). Another difference between our system and SAR is that our detector (the human eye) is an incoherent imaging device, being sensitive to only the intensity of the incoming light. This characteristic of the eye prevents the synthetic apertured hologram from displaying superresolved images, as is the case for SAR.

Vertical deflection is provided by a closed-loop galvanometric scanner. The net effect is that of a small horizontal-parallax hologram being scanned in a raster fashion, much like the electron beam in a CRT display.<sup>7,8</sup> History-minded readers may note that the display exhibits many similarities to the Scopony system introduced in the 1930's for the projection of television images.<sup>9,10</sup>

Computation of the images is done on a massively parallel supercomputer (Thinking Machines Corporation Model CM2) that uses algorithms developed at our laboratory. The description of those computational techniques is outside the scope of this paper, and the interested reader is referred to a companion paper for details.<sup>11</sup> After computation the holographic information is sent to a high-resolution frame buffer and converted to a signal with the same bandwidth as the AOM. This signal is then upconverted to the AOM operating frequency range by being mixed with a 100-MHz carrier and filtered to keep only the lower sideband. It is then amplified and used to drive the AOM.

The operation of the display requires a precise synchronization among the various parts of the system (polygonal mirror, galvanometric mirror, and frame buffer), which is provided by the circuit of Fig. 2. This circuit derives all the necessary drive signals from the horizontal and vertical sync pulses of the frame buffer.

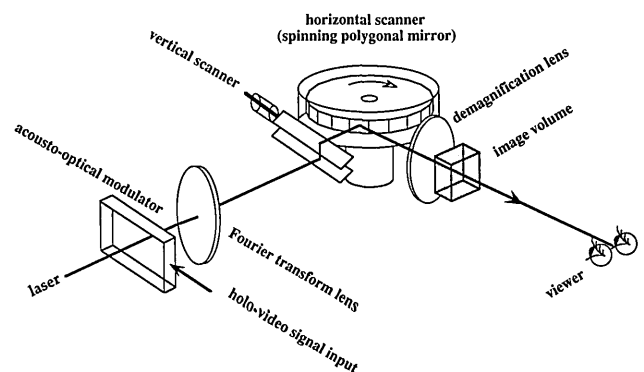


Fig. 1. Schematic view of the MIT electronic holography display.

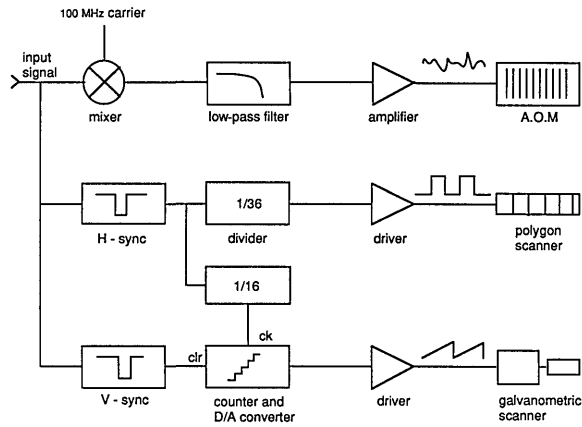


Fig. 2. Holographic display signal processing: D/A, digital-to-analog.

### 4. MATHEMATICAL OPTICS OF THE SYNTHETIC APERTURE DISPLAY

#### A. AOM as a Dynamic Hologram

Because of their wide bandwidth and dynamic range, Bragg cells have found many applications as elements of optical processors.<sup>12,13</sup> The optical processing community usually uses the formalism of linear systems theory to describe the operation of these devices. It will be much easier in the course of this section to treat the signal propagating on the AOM as a dynamic hologram rather than as an arbitrary waveform. This description also closely corresponds to the actual physical phenomenon we are trying to reproduce, namely, three-dimensional imaging. Let us say that the object we want to display is a single point. At the computation step the corresponding geometry is shown in Fig. 3. The hologram plane is at a distance  $h_0$  from point  $P_0$ , and the simulated wavelength corresponds to the wavelength eventually used for display (usually 633 nm). The maximum spatial frequency of the fringes is related to the maximum viewing angle by Eq. (1). During playback, the hologram information is launched at one end of the crystal as a series of rf shear waves. The wavelength  $\lambda_{\text{sound}}$  of these waves is related to the speed of sound  $v_s$  of the crystal and the rf frequency  $F$  by the equation

$$\lambda_{\text{sound}} = v_s/F. \tag{6}$$

Usually  $\lambda_{\text{sound}}$  is longer than the original fringe spacing  $\lambda_{\text{fringe}}$ . The playback hologram will thus have correspondingly lower spatial frequencies with the following consequences:

- (1) The holographic image will be magnified along the  $x$  axis by a factor equal to  $\lambda_{\text{sound}}/\lambda_{\text{fringe}}$ .
- (2) The maximum view angle will be reduced by the factor  $\lambda_{\text{sound}}/\lambda_{\text{fringe}}$ .
- (3) The image will be magnified along the  $z$  axis by the factor  $(\lambda_{\text{sound}}/\lambda_{\text{fringe}})^2$ .
- (4) The image will be at a distance  $d_0 = h_0 (\lambda_{\text{sound}}/\lambda_{\text{fringe}})^2$  from the crystal plane.
- (5) The image will move along the  $x$  axis at the speed  $v_s$ .

Because the longitudinal and transverse magnifications are different, the image will exhibit some distortion since

it is elongated along the axis of highest magnification. For example, a sphere will be mapped into an ellipsoid.

#### B. Horizontal Scanning: Geometric Analysis

##### 1. Scanning in the Focal Plane

First we analyze the case in which the polygonal mirror is in the focal plane of lens  $L_1$  (Fig. 4). This also corresponds to the original Scopphony design. Let  $v_s$  be the speed of shear waves on the AOM crystal,  $\omega$  be the angular speed of the polygon, and  $\theta$  be the angle scanned by the polygon. For the waves on the AOM to appear stationary when seen reflected by the mirror we must have

$$\omega = -\frac{1}{2} \frac{d\theta}{dt} = -\frac{v_s}{2f_1}, \tag{7}$$

where  $f_1$  is the focal length of lens  $L_1$  and  $t$  is the time. The factor of 2 in Eq. (7) comes from the fact that the angle of deflection is twice the mirror's rotation. In practice,  $\omega$  is determined by the scan time  $\tau$  of a single holographic line by the relation

$$\omega = \frac{2\pi}{N\tau}, \tag{8}$$

where  $N$  is the polygon's number of facets. The distance  $f_1$  between the polygon and the AOM is, thus, simply

$$f_1 = \frac{v_s N \tau}{4\pi}. \tag{9}$$

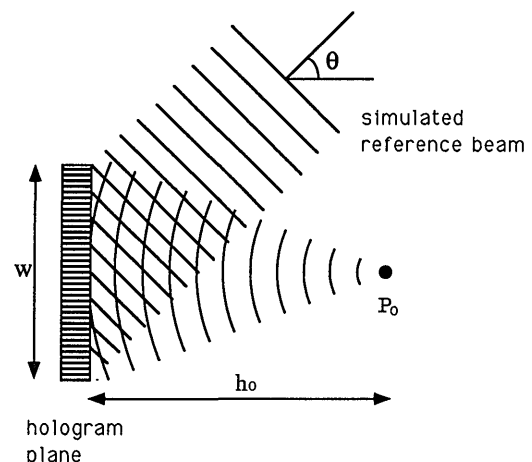


Fig. 3. Hologram geometry for the computation of a single point.  $\theta$  is the simulated reference beam angle. The fringe pattern is sampled at the hologram plane.

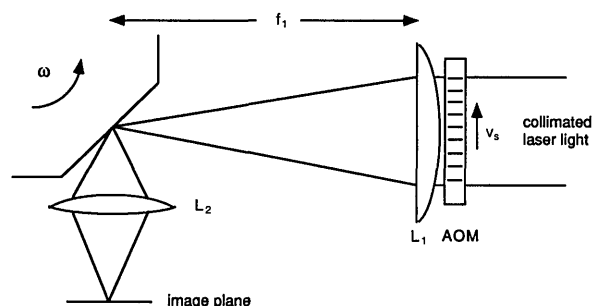


Fig. 4. Horizontal scanning geometry for the focal scanning case. The vertical scanning optics are not shown for clarity.  $L_1$  is a cylindrical lens.

The angular deflection of the AOM is usually not large enough for viewing, so we increase it by using a second lens,  $L_2$ , in a telescopic configuration with  $L_1$ . In this case, the view angle is multiplied by a factor  $K$  that is equal to the inverse of the telescope's transverse magnification  $M_t$ :

$$K = 1/M = f_1/f_2, \tag{10}$$

where  $f_2$  is the focal length of lens  $L_2$ . The longitudinal magnification  $M_l$  of the system correspondingly becomes

$$M_l = M_t^2 = (f_2/f_1)^2. \tag{11}$$

If we choose lens  $L_2$  so that its focal length satisfies the condition

$$f_1/f_2 = \lambda_{\text{sound}}/\lambda_{\text{fringe}}, \tag{12}$$

the telescopic magnification of the lens system will be the inverse of the magnification described in Subsection 3.A and the computed object will be displayed with no distortion.

Equations (7)–(9) are valid regardless of the holographic image's position with respect to the AOM because the horizontal scanning plane coincides with the focal plane of lens  $L_1$ . We might now ask ourselves what would happen if this condition were not fulfilled, i.e., if the scanning plane and the focal plane were different.

### 2. Nonfocal Scanning

We now investigate the configuration shown in Fig. 5. We see that the focal plane of lens  $L_1$  and the scanning surface no longer coincide. We continue to consider our holographic image as consisting of a single point  $P_0$  floating at a distance  $d_0$  from the plane of the AOM. Equivalently, we can think of the series of corresponding fringes launched on the crystal as a Gabor zone lens, i.e., as a lens with a focal length  $d_0$ . As a convention we consider  $d_0$  to be positive if the holographic image is virtual, as shown in Fig. 5. For simplicity we also consider the distance between the AOM and  $L_1$  to be negligible. After the action of lens  $L_1$ , the distance  $d_i$  between the AOM and the new image  $P_i$  is given by the Gaussian lens formula

$$1/f_1 = 1/d_0 + 1/d_i. \tag{13}$$

$P_0$  translates along the  $x$  axis with a velocity equal to the speed of the shear waves in the AOM. Thus the speed  $v_i$  at which the image  $P_i$  moves along the  $x$  axis is related to the speed of sound  $v_s$  in the crystal by the relation

$$v_i = M_{ti}v_s = \frac{-v_s(d_i - f_1)}{f_1}, \tag{14}$$

where  $M_{ti}$  represents the lateral magnification resulting from the imaging action of  $L_1$ .

For the image to look stationary when reflected from the polygon, it must satisfy a relation analogous to Eq. (7), that is,

$$\frac{v_i}{2\omega} = D - d_i, \tag{15}$$

where  $D$  is the distance between the AOM and the horizon-

tal scanning plane. Combining Eqs. (13)–(15) then leads to the equation

$$\frac{f_1 v_s}{2\omega} + D(d_0 - f_1) - f_1 d_0 = 0. \tag{16}$$

Equation (16) demonstrates that the scanning plane and the focal plane of  $L_1$  need not coincide and thus provides an additional degree of freedom to the designer. Indeed, Eq. (7) can be thought of as a special case of Eq. (16) corresponding to  $D = f_1$ .  $L_1$  and  $L_2$  are still in a telescopic configuration, so Eqs. (10)–(12) can be applied. A few comments are useful here. First, Eq. (16) is valid over a wide range of conditions;  $d_i$  can be either positive (e.g., the holographic image is virtual) or negative (the real-image case). The rotational direction of the polygon can be inverted and an image will still be presented, provided that Eq. (16) is satisfied. This rather counterintuitive aspect of Eq. (16) has been confirmed experimentally. Second, Eq. (16) is valid for only one value of  $d_i$  once the other parameters have been fixed. This will result in a motion-blurred image at hologram planes other than  $d_i$ .

While this effect may seem rather inconvenient at first, it is useful if the holographic information contains artifacts, such as narrow gaps. In that case, the gaps can become so blurred as to be hardly noticeable. Use of the conditions of Eq. (7) would make these gaps as visible as the hologram itself, giving the user the impression that the image is viewed through a picket fence. The price is, of course, a limited useful image depth.

### C. Horizontal Scanning: Spatial Frequency Analysis

Another successful approach to the analysis of the display comes from the use of Fourier optics. We now describe the display as a linear system into which information is fed as an rf signal and converted to a range of spatial frequencies. A necessary condition for the faithful reproduction of the CGH is that the spatial bandwidth of the display be larger than the bandwidth of the input signal.

The first stage in our display is the conversion of an rf signal to an optical wave front. The spatial frequency range of the acoustic fringes (and, thus, of the phase-modulated wave front) is simply

$$\Delta f_s = \frac{\Delta\nu}{v_s}, \tag{17}$$

where  $f_s$  denotes the spatial frequencies,  $\Delta\nu$  is the rf range, and  $v_s$  is the acoustic velocity.

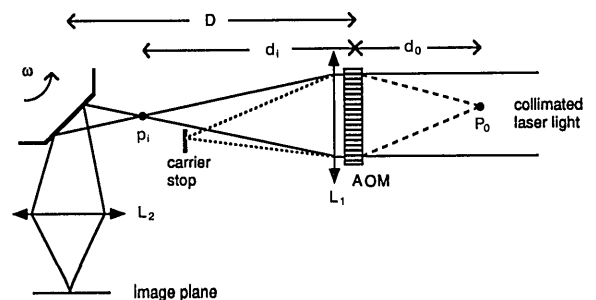


Fig. 5. Horizontal scanning geometry for the nonfocal scanning case.  $P_0$  is the virtual image created by the fringe pattern on the AOM.

For the rest of this analysis we consider the case in which the horizontal scanning plane and the focal plane coincide. We have a Fourier transform of the AOM spatial frequencies at the scanning plane, of size

$$\Delta x = \lambda D \Delta f_s = \lambda D \frac{\Delta \nu}{v_s}, \quad (18)$$

where  $\lambda$  is the wavelength of the laser light. Using Eq. (9) then gives the result

$$\Delta x = \frac{N \tau \lambda \Delta \nu}{4\pi}. \quad (19)$$

It is interesting to note here that the size of the Fourier transform is independent of the speed of sound in the crystal. One might now ask, How are the polygon's parameters related to the desired image characteristics? The number of resolvable points of any scanning system is given by its time-bandwidth product.<sup>14</sup> In the case of the polygon this is simply expressed as

$$N_{\text{res}} = \frac{W\theta}{a\lambda}, \quad (20)$$

where  $\theta$  is the optical deflection angle,  $W$  is the beam size, and  $a$  is an aperture shape factor (typically  $1 < a < 3$ ). For the polygon to reproduce the holographic image faithfully,  $N_{\text{res}}$  must be greater than the time-bandwidth product of an entire holographic line, i.e.,

$$\frac{W\theta}{\lambda} \geq \tau \Delta \nu, \quad (21)$$

where we have set the aperture factor to 1 (which corresponds to the case of uniformly illuminated rectangular aperture).  $W$  is equivalent to  $\Delta x$  of Eq. (19) if the scanning is done in the Fourier plane. We now introduce a retrace interval  $\tau_r$  at the end of each displayed line. This retrace interval is just a blank space and contains no information. Inequality (21) now becomes

$$\frac{\Delta x \theta}{\lambda} \geq \tau_a \Delta \nu, \quad (22)$$

where

$$\tau_a = \tau - \tau_r \quad (23)$$

is the active or nonblank interval.

We note that  $\theta$  corresponds to the deflection range over which the full Fourier transform fits on a facet. In the case of a polygon scanner, the facet boundaries move across the Fourier transform as the polygon scans angularly, resulting in a smaller effective deflection angle if we want the full Fourier transform to be scanned at any one time. It can be shown that this effective deflection angle is given by the formula

$$\theta_{\text{eff}} = \frac{4\pi}{N} - 4 \tan^{-1} \left( \frac{\Delta x}{2R} \right), \quad (24)$$

where  $R$  is the polygon's radius. Using inequality (22) and Eq. (24) results in the inequality

$$\frac{4\pi}{N} - 4 \tan^{-1} \left( \frac{\Delta x}{2R} \right) - \frac{\lambda \tau_a \Delta \nu}{\Delta x} \geq 0. \quad (25)$$

In most cases,  $\Delta x \ll 2R$ , so we can use the approximate form of inequality (25):

$$\frac{4\pi}{N} - \frac{2\Delta x}{R} - \frac{\lambda \tau_a \Delta \nu}{\Delta x} \geq 0. \quad (26)$$

Using Eq. (19) as our expression for  $\Delta x$  and Eq. (23) as our expression of  $\tau$ , we obtain the following equation after a few manipulations:

$$\tau_r - \frac{(\tau_a + \tau_r)^2 \lambda N^2 \Delta \nu}{8\pi^2 R} \geq 0. \quad (27)$$

We now want to solve inequality (27) for  $\tau_r$ , so by rearranging the terms we arrive at the second-degree expression:

$$k\tau_r^2 + (2k\tau_a - 1)\tau_r + k\tau_a^2 \geq 0, \quad (28)$$

where we have set

$$k = \frac{\lambda N^2 \Delta \nu}{8\pi^2 R}. \quad (29)$$

This second-degree expression has real roots if the following condition is met:

$$1 - 4k\tau_a \geq 0, \quad (30)$$

which is equivalent to requiring that

$$R \geq \frac{\lambda N^2 \tau_a \Delta \nu}{2\pi^2}. \quad (31)$$

The retrace interval  $\tau_r$  is at a minimum when we have an equality in expression (31), and  $\tau_r$  is then

$$\tau_r = \tau_a. \quad (32)$$

Expression (31) and Eq. (32) give the minimum acceptable polygon radius and retrace interval for obtaining perfect imaging of a hologram. Equations (8), (9), and (32) and expression (31) then completely specify the system in the case of Fourier plane scanning. We can now compute the characteristics of lens  $L_2$ : Its focal length is dictated by Eq. (12) and its minimum diameter  $P$  is given by

$$P = 2f_2 \tan \left( \frac{\theta_{\text{eff}}}{2} \right) + \Delta x. \quad (33)$$

The choice of the correct parameters is now a matter of engineering choices: a polygon with a higher number of facets will rotate more slowly and will require higher  $f$ -number optics but will be much bigger, heavier, and more expensive. Reducing the number of facets rapidly leads to impractical output lens  $f$ -number values. Increasing the retrace time alleviates these problems but will result in an unacceptable refresh rate for a single acoustic channel.

#### D. Display Resolution

At any instant in time only a small portion of the image will be displayed. From the viewer's perspective the display can be modeled as a narrow aperture being rapidly scanned across a larger hologram (Fig. 6). It is clear that this narrow aperture, which is also the output pupil, consists of the image of the AOM formed by lenses  $L_1$  and  $L_2$

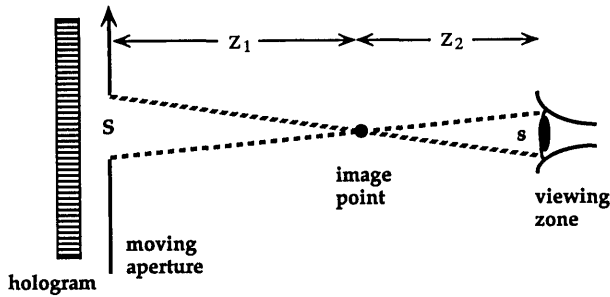


Fig. 6. Apertured modulator.

of Fig. 4. The maximum useful display resolution is determined by the pupil of the observer. If we assume a diffraction-limited system and consider an instant in time in which the diffracted light entirely fills the pupil of the viewer, the maximum resolution condition is given by

$$\frac{z_1}{S} < \frac{z_2}{s}, \tag{34}$$

where  $S$  is the size of the AOM image and  $s$  is the diameter of the eye pupil (Fig. 6). In practice, condition (34) cannot be met because the aperture scans across the image and part of the subtend of the eye's pupil will be blocked during a fraction of the scan. The time behavior of the display resolution for a given image location will exhibit the behavior shown in Fig. 7. Since the scan time is much smaller than the response time of the eye, the resolution function of Fig. 7 is integrated over time by the visual system with the result that the overall resolution will always be inferior to the diffraction limit of the eye, although approaching it asymptotically as  $S$  becomes large. In practice, however, a determination of  $S$  from inequality (34) gives visually excellent results. It is also obvious from inequality (34) that the deeper the image, the longer the AOM has to be. The actual size of the AOM can be expressed as

$$S > \frac{\Delta z s}{M(z_{\text{obs}} - \Delta z)}, \tag{35}$$

where  $z_{\text{obs}}$  is the distance between the observer and the AOM image, which is usually close to the output lens,  $\Delta z$  is the maximum depth of the image (assuming that the hologram lies entirely in front of the AOM), and  $M$  is the magnification factor of Eq. (10). As an example, with  $M^{-1} = 5$  (corresponding to a view zone with a  $14.5^\circ$  angular width and assuming a 50-MHz bandwidth  $\text{TeO}_2$  AOM),  $\Delta z = 100$  mm,  $s = 3$  mm, and a viewing distance of 600 mm, the minimum required AOM length is 3 mm, which corresponds to a space-bandwidth product of 243. Such a figure is well within the range of commercially available  $\text{TeO}_2$  AOM's, since some of these exhibit space-bandwidth figures in the thousands.<sup>15,16</sup> For all practical purposes, the display resolution will thus be limited generally by the quality of the system optics or by the algorithms used in the hologram computation.

**E. Vertical Scanning**

The vertical scanning section of the system is more straightforward because our display exhibits no vertical parallax. The vertical scanning is effected in a raster fashion, and its rate (typically from 30 to 60 Hz) places it

well within the range of commercially available closed-loop galvanometric scanners.<sup>14</sup> Moreover, the required vertical resolution is relatively low (fewer than 1000 lines) and remains well within the modulation transfer function limits of ordinary scanning lenses. Because the vertical focal plane is fixed and the horizontal focus is variable, deep images will exhibit some astigmatism, as they do in any horizontal parallax-only autostereoscopic display.<sup>6</sup> This astigmatism can be kept to a minimum if the vertical focal plane coincides with the middle plane of the image. Extensive experience with rainbow holograms shows that this astigmatism remains almost unnoticeable, even for fairly deep objects.

A desirable feature of the vertical scanning system is that the output beam be normal to the image plane throughout the field. This condition, known as telecentricity, ensures that the displayed image will not become vertically distorted as the horizontal focus is moved away from the vertical focus plane. A telecentric system converts an angular beam deflection to a linear translation by having the scanning element positioned 1 focal length in front of the output lens.<sup>17</sup> This causes a problem in our system since this space is usually occupied by the horizontal scanning polygon. The solution is to put the vertical scanner away from the polygon and reimage it at the required plane by using a cylindrical relay lens  $L_3$  (Fig. 8). We can then use the same lens  $L_2$  as both a horizontal and a vertical output lens. The geometry of the vertical scanning subsystem results in a narrow viewing zone, and it is usually necessary to place a one-dimensional diffuser in the vertical focus plane.<sup>18</sup> Such a diffuser can be approximated by a fine-pitched lenticular array or can be produced by holographic techniques.<sup>18</sup> Placing the diffuser in the vertical focus plane of the display increases the view zone by diffusing each line in the vertical direction but leaves the horizontal image content unaltered.

**5. SIGNAL PROCESSING**

The display apparatus consists of CGH generation and storage, data transmission, and electro-optic display subsystems. A synthetic three-dimensional object is constructed by using standard three-dimensional graphics and animation editing methods. Data describing the object are transferred to the Thinking Machines Connection Machine Model 2 (CM2) minisupercomputer, which contains 16,384 microprocessors in a massively parallel hypercube processing architecture. The computation of the holographic information itself is beyond the scope of this paper; the algorithms used by the MIT group will be published in a subsequent paper.<sup>11</sup>

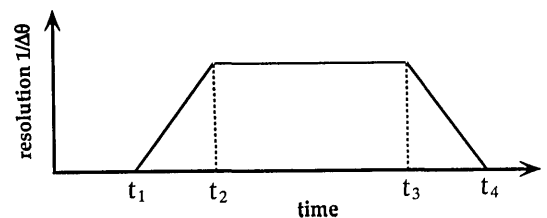


Fig. 7. Display resolution time dependence for a stationary observer. The diffracted rays are vignetted by the observer's pupil during intervals  $t_1 - t_2$  and  $t_3 - t_4$ .

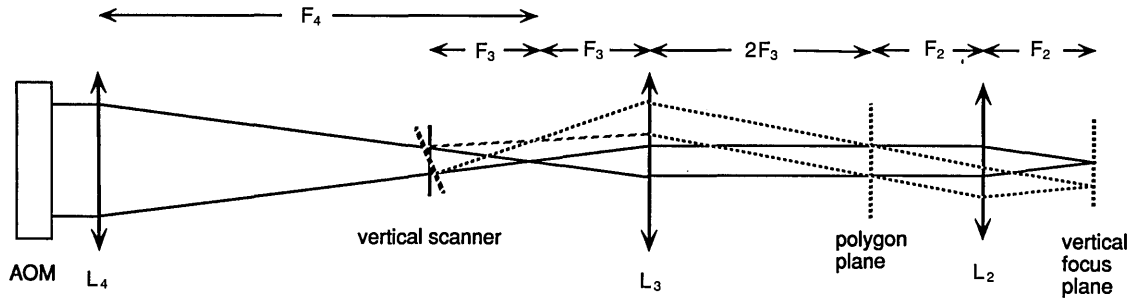


Fig. 8. Vertical scanning geometry for a single-channel AOM. The output lens  $L_2$  is the same as in Figs. 4 and 5.  $L_3$  and  $L_4$  are cylindrical.

The CM2 calculates a single frame of the CGH, which consists of a complex series of sinusoidal variations, and loads this fringe pattern into its frame buffer. The frame buffer is configured to store and read out the CGH as 64 horizontal lines, each of which consists of 32,768 data points (video pixels). All commercially available frame buffers include a retrace interval between video lines during which the signal is blanked so that gaps will be included in the signal fed to the display. The effect of these blank intervals is that the hologram will look as if it is being viewed through a picket fence. This effect can be greatly attenuated by using the configuration of Fig. 5, as explained in Section 4, which positions the gaps well behind the hologram image. The picket fence will be motion blurred, and the image becomes much more satisfying to the eye. A custom-built frame buffer able to generate single continuous lines would, of course, eliminate this problem and greatly improve the image quality at extreme depth.

The fringe pattern is transmitted from the frame buffer to the display as a 50-MHz bandwidth video signal that propagates over an optical-fiber link. An optical receiver sends the video signal to the display electronics (see Fig. 2). The link also transmits the necessary synchronization signals, which are separated by the display electronics and processed into control signals for the optomechanical scanning portion of the display apparatus. The video signal is then mixed with a 100-MHz carrier and filtered to keep only the lower sideband. This upconverts it to the 50–100 MHz operating range of the AOM. The signal is then amplified and used to drive the AOM.

### 6. USE OF MULTICHANNEL AOM'S

Increasing the view zone or the size of the display by a certain factor while keeping the refresh rate constant requires a proportionally larger number of samples per unit time. For a single acoustic channel, this translates into a larger operating bandwidth for both the AOM and the associated electronics. A more elegant approach is to use a multichannel AOM, thus making use of the parallelism inherent in optical systems. Such an approach has been used extensively by the signal processing community,<sup>19,20</sup> and devices with low cross talk between channels and high space-bandwidth products are readily available. By using a three-channel AOM and the red, green, and blue output of the CM2 frame buffer it becomes possible to triple the vertical resolution for a total of 192 lines. Our multichannel modulator also uses  $\text{TeO}_2$  in the shear mode and consists of three acoustic channels with an individual

width of 3.2 mm and an interchannel spacing of 1.5 mm. The cross talk is specified to be better than 25 dB across an aperture of  $20 \mu\text{s}$ . Because the acoustic channels are large and well separated it was found to be necessary to optically multiplex the corresponding holographic lines with a simple holographic optical element (HOE) consisting of three gratings with the same spatial frequencies<sup>18</sup> (Fig. 9). The first two gratings,  $G_1$  and  $G_2$ , diffract the outer lines in the +1 and -1 orders, respectively, while the effect of  $G_3$  is to recombine the beams. The multiplexed lines are then processed in a fashion identical to the description given in Section 5 (Fig. 10). Our experiments utilized gratings made by bleaching recordings in silver halide emulsions.

### 7. RESULTS

The system described in Subsection 4.B.2 was built and tested with excellent results. The displayed images proved to be crisp, with a high contrast and an acceptable depth of field of  $\sim 3 \text{ cm}$ , although their vertical resolution was limited to 64 lines (Fig. 11). The depth-of-field limitation arose from the reduction of the picket fence effect by motion blurring, as described above. Future frame buffers designed to be free of blanking intervals should permit the display of much deeper images. The calculation time of a wire frame CGH on the CM2 ranged from 0.3 to 10 s, depending on the complexity of the image, and by precomputing a set of frames and playing them back from the RAM memory of the CM2 we were able to achieve a frame rate of  $\sim 8$  images per second. We were also able to file such animated sequences in the CM2 Datavault for subsequent playback. The image size was  $\sim 5 \text{ cm} \times 3 \text{ cm}$  for a view angle of  $15^\circ$ . As described in Section 4.C, the images exhibited some brightness falloff at the image sides because of the absence of a programmable horizontal retrace interval, but this effect remained visually acceptable.

The 192-line display also gave excellent results, although it exhibited a somewhat lower signal-to-noise ratio. The

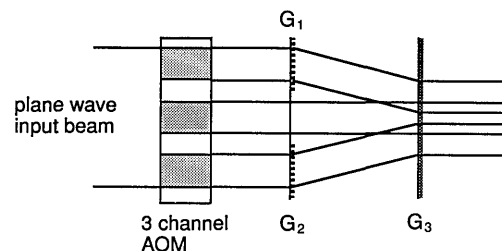


Fig. 9. Three-channel AOM and holographic beam multiplexer.

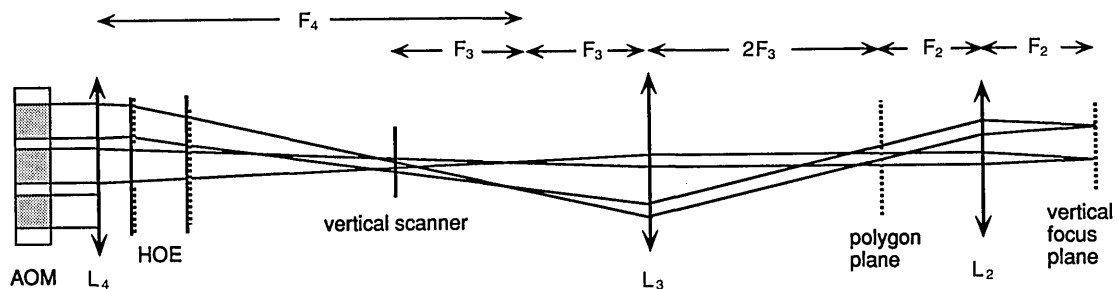


Fig. 10. Vertical scanning geometry for a three-channel AOM.

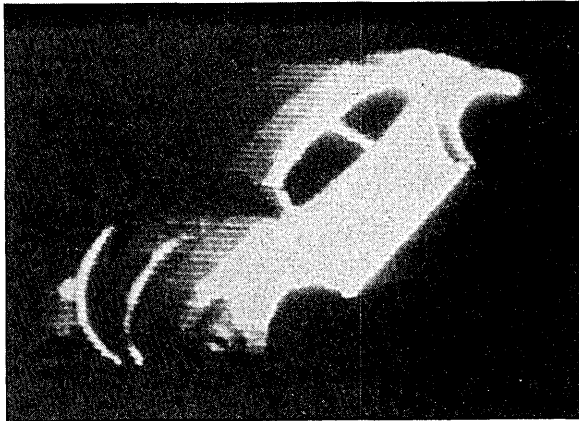


Fig. 11. Shaded image displayed by the MIT system.

principal source of noise in this case was identified as light scattering from the multiplexing HOE. Using higher performance materials (such as dichromated gelatin or photopolymer) for the gratings would considerably reduce this scattering noise. The interchannel cross talk was visually unnoticeable.

## 8. FUTURE DIRECTIONS

### A. Higher Bandwidth Crystals

As demonstrated in Section 5, using higher bandwidth AOM crystals can result in significantly more complex images. Longitudinal mode  $\text{TeO}_2$  modulators are particularly attractive in this respect because their bandwidth matches the frequency range of today's top-of-the-line frame buffers ( $\sim 200$  MHz). Longitudinal  $\text{TeO}_2$  AOM's are also a relatively mature technology, and several manufacturers offer products with suitable time-bandwidth products. Another advantage of this material is the possibility of packing a large number of acoustic channels into a small space without excessive cross talk. Channel spacing of less than  $250 \mu\text{m}$  has been reported.<sup>20</sup>

### B. Electronic Hardware

Commercially available frame buffers are poorly suited to drive a device such as this synthetic aperture display. Their main limitation comes from the limited number of samples available between horizontal blanking intervals, which results in the picket fence effect mentioned above. The ideal device would be capable of outputting uninterrupted sample streams of arbitrary length and would include a programmable retrace interval at the end of each such sequence. Of course the output bandwidth should be

compatible with the type of AOM specified in the design, and the buffer RAM should be larger than today's frame buffers (between 2 and 10 Mbytes per channel, depending on the type of AOM). Since any practical holographic display device is likely to include a large number of acoustic channels, the frame buffer should be easily expandable and software reconfigurable. The input bandwidth should be as large as possible to allow for a reasonable frame rate.

### C. New Horizontal Scanning Technologies

According to inequality (31), using a polygonal mirror scanner as our horizontal scanning elements results in an unreasonable polygon size for any display of significant dimensions. We are investigating the use of different technologies, such as arrays of high-speed galvanometric scanners, to circumvent that problem.

## 9. CONCLUSION

We have demonstrated a new method of displaying holographic information at video refresh rates by using a combination of AO and electromechanical laser scanning technologies. Although the displayed images are small, they are bright, have good resolution, and exhibit all the depth cues found in conventional holography. Much larger displays should be realizable by using currently available technologies, although these represent a major challenge from an engineering point of view. Our results show that the promise of real-time holography is becoming a reality.

## ACKNOWLEDGMENTS

The work described here was sponsored by US WEST Advanced Technology, Inc., the Defense Advanced Research Projects Agency, through the Rome Air Development Center (contract F30602-89-C0022), and the Television of Tomorrow research consortium of the MIT Media Laboratory. We thank John Earls, Jim Salem, and David Shepard of Thinking Machines Corporation for their help in adapting the CM2 frame buffer to our purposes.

## REFERENCES

1. W. J. Dallas, "Computer generated holograms," in *The Computer in Optical Research*, B. R. Frieden, ed., Vol. 41 of Springer Series in Applied Physics (Springer-Verlag, Berlin, 1980), pp. 291-366.
2. G. Tricoles, "Computer generated holograms: a historical review," *Appl. Opt.* **26**, 4351-4360 (1987).
3. E. Leith, J. Utpatnieks, K. Hildebrand, and K. Haines,

- "Requirements for a wavefront reconstruction television facsimile system," *J. SMPTE* **74**, 893–896 (1965).
4. L. H. Enloe, J. A. Murphy, and C. B. Rubinstein, "Hologram transmission via television," *Bell Syst. Tech. J.* **1**, 335–339 (1966).
  5. C. B. Burckhardt and L. H. Enloe, "Television transmission of holograms with reduced resolution requirements on the camera tube," *Bell Syst. Tech. J.* **4**, 1529–1535 (1969).
  6. S. A. Benton, "The mathematical optics of white light transmission holograms," presented at the First International Symposium on Display Holography, Lake Forest College, Lake Forest, Ill. (1982).
  7. P. St. Hilaire, S. A. Benton, M. Lucente, M. L. Jepsen, J. Kollin, and H. Yoshikawa, "Electronic display system for computational holography," in *Practical Holography IV*, S. A. Benton, ed., *Proc. Soc. Photo-Opt. Instrum. Eng.* **1212**, 174–182 (1990).
  8. S. A. Benton, "Experiments in holographic video," in *Holography*, P. Greguss and T. H. Jeong, eds., *Proc. Soc. Photo-Opt. Instrum. Eng.* **IS08**, 247–267 (1991).
  9. L. M. Myers, "The Scopony system: an analysis of its possibilities," *TV Shortwave World* (1936), pp. 201–294.
  10. A. Korpel, R. Adler, P. Desmares, and W. Watson, "A television display using acoustic deflection and modulation of coherent light," *Appl. Opt.* **5**, 1667–1682 (1966).
  11. M. Lucente, "Optimization of hologram computation for real time display" in *Practical Holography VI*, S. A. Benton, ed., *Proc. Soc. Photo-Opt. Instrum. Eng.* **1667** (to be published).
  12. A. Goutzoulis and I. Abramovitz, "Digital electronics meets its match," *IEEE Spectrum* **25**(8), 21–25 (1988).
  13. N. J. Berg and J. N. Lee, eds., *Acousto-Optic Signal Processing Theory and Implementation*, Vol. 2 of Optical Engineering Series (Dekker, New York, 1983).
  14. L. Beiser, "Laser scanning systems," in *Laser Applications* (Academic, San Diego, Calif., 1974), Vol. 2, pp. 53–155.
  15. I. C. Chang, "Acoustooptic devices and applications," *IEEE Trans. Sonics Ultrason.* **SU-23**, 2–22 (1976).
  16. A. Korpel, "Acousto-optics—a review of fundamentals," *Proc. IEEE* **69**, 48–53 (1981).
  17. R. E. Hopkins and M. J. Buzawa, "Optics for laser scanning," *Opt. Eng.* **15**, 90–94 (1976).
  18. P. St. Hilaire, S. A. Benton, M. Lucente, J. Underkoffler, and H. Yoshikawa, "Real-time holographic display: improvements using a multichannel acousto-optic modulator and holographic optical elements," in *Practical Holography V*, S. A. Benton, ed., *Proc. Soc. Photo-Opt. Instrum. Eng.* **1461**, 254–261 (1991).
  19. L. Bademian, "Parallel-channel acousto-optic modulation," *Opt. Eng.* **25**, 303–308 (1986).
  20. A. VanderLugt, G. S. Moore, and S. S. Mathe, "Multichannel Bragg cells: compensation for acoustic spreading," *Appl. Opt.* **22**, 3906–3912 (1983).